F

Engineering and Technology

AERODYNAMIC DRAG REDUCTION OF A GENERIC LORRY MODEL USING CONTINUOUSLY BLOWING JETS

Peerapong Kumkhuntod[1] and Kamthon Septham[2*]

[1,2]Department of Mechanical Engineering, Faculty of Engineering,
King Mongkut's University of Technology Thonburi, Thailand
***Corresponding author, E-mail:** kamthon.sep@mail.kmutt.ac.th

Abstract

Aerodynamic drag reduction is one of the available techniques to reduce energy consumption and greenhouse gas emissions from the road transport sector. In the present study, the squared-back Ahmed body, representing the generic model of a lorry, is investigated. Continuously blowing jets, were installed at the top of the rear part of the squared-back Ahmed body to alter wake structures behind it. The drag-reducing mechanisms using continuously blowing jets were identified. Numerical simulations of airflow over the Ahmed body at Re_H = 33,000 were carried out using OpenFOAM. The results show that the drag coefficient of the squared-back Ahmed body for uncontrolled flow agrees well with the literature value. For controlled flow, six different cases were investigated based on the magnitude of the jet velocity at 20%, 40%, 50%, 60%, 80%, and 100% of the free-stream velocity, U_∞, respectively. It shows that the optimum drag coefficient C_d can be achieved when the continuously blowing jet velocity is approximately equal to $0.6U_\infty$. The corresponding drag reduction of 3.81% is reached; the mean base pressure recovery of 8.76% is obtained. In addition, the correlation between an increasing recirculation length and a base pressure recovery is established.

Keywords: Aerodynamics, Drag Reduction, Ahmed Body, Flow Control, Computational Fluid Dynamics

Introduction

Road transport is one of the major contributors to greenhouse gas emissions (IPCC, 2014). Nowadays, lorries are widely used for cargo transport. Several efforts are currently being invented to reduce greenhouse gas emissions into the atmosphere, such as the use of alternative energy propulsion systems, the implementation of low-emission combustion technologies, etc. In terms of aerodynamics, a lorry can be categorized as a bluff body or a blunt body. Lorries have an inevitable loss of energy caused by air resistance in terms of form drag during being driven forward.

There are several flow control techniques to reduce form drag (Barros et al., 2016). Typically, flow control techniques can be divided into two categories based on energy expenditure: passive control and active control (Gad-el-Hak, 2000). Passive control is mainly related to shape modifications; energy expenditure is not required to activate actuators. Since most lorries are legally restricted in terms of size and shape modifications that could pose a danger to road users and reduce the payload capacity, it is not possible to significantly modify the shapes of a lorry. Therefore, active control, using blowing, suction, and synthetic jet actuators, becomes more attractive than passive control since no significant shape modifications are needed. This paper focuses on numerical studies of aerodynamic drag reduction of a generic lorry model by means of continuously blowing jets installed at the top of the rear part of a lorry to alter wake structures behind it. In this study, a better

understanding of the physics of fluid flow around a bluff body with enhanced active control conditions and their effect on the force and base pressure coefficients is provided.

Research Objectives

1. To investigate the drag-reducing mechanisms by means of continuously blowing jets, installed at the top of the rear part of the squared-back Ahmed body, a generic lorry model.
2. To quantify the optimum drag coefficient by varying the magnitude of the jet velocity.

Literature Review

The aerodynamic resistance acting on a lorry is opposite to the direction of motion. In general, the main aerodynamic resistance on a generic lorry occurs in four main areas: the frontal area, the gap between a roof cab and a trailer, the underbody, and the rear part of a trailer (Bradley, 2000). Form drag (or boundary-layer pressure drag) is considered to be a significant portion of the total aerodynamic drag acting on a lorry. It primarily depends on the shapes of a lorry; it is caused by the boundary-layer separation from the surface at the rear part of a trailer.

In 1984, the "Ahmed body" was first introduced to investigate the characteristic features of the flow around a ground vehicle (Ahmed, Ramm, & Faltin, 1984). Then, it has been widely used as a standard model for analyzing road vehicle aerodynamics. Its shape is 1.044 meters long, 0.288 meters tall, 0.389 meters wide, and is attached to four 0.5 meters cylindrical stands located at the base. Typically, flow structures behind the Ahmed body are composed of vortices, recirculation regions, separation bubbles, and reattachment zones. It is suggested that the slant angle at the rear of the body significantly affects the drag coefficient.

Flow control for drag reduction of lorries involves both passive and active techniques based on energy expenditure. Several flow control strategies are introduced to suppress the form drag of the bluff body (Barros, Borée, Noack, Spohn, & Ruiz, 2016). The goal is either to reduce wake entrainment, to elongate the formation region towards the Kirchhoff flow, to decrease the cross-section of the wake in order to modify the bubble's aspect ratio, or to recover static pressure at the rear of the body (Roshko, 1995; Gerrard, 1996). These drag-reducing techniques are interesting because there is no need to modify the body itself which may decrease the payload capacity of lorries. Physical mechanisms related to drag reduction have also been investigated. It shows that the symmetry and stability of a wake depend on the Reynolds number (Grandemange, Cadot, & Gohlke, 2012). The reflectional symmetry-breaking regime is permanent at high Reynolds numbers. Feedback control for a low Reynolds regime and open-loop control for a high Reynolds number regime have been studied to reduce the form drag of a squared-back Ahmed body (Evstafyeva, 2018). Clapperton (2017) employed continuously blowing jets to reduce drag inflow passing a circular cylinder in the subcritical Reynolds number flow regime. It is suggested that streamwise vortices, shed into the separating shear layer due to the interaction between the jets and cross-flow, form positive drag reducing mechanisms.

Methodology

The processes of numerical simulations in this study were divided into four main parts as follows:

Part 1: Define the computational domain.
Part 2: Define the boundary conditions, properties of fluid, and parameters.
Part 3: Generate a mesh of the fluid domain.
Part 4: Perform the simulations and investigate the results.

Part 1: Define the Computational Domain

The size of the fluid domain and model are defined according to the suggestions from ERCOFTAC (Evstafyeva, 2018; Manceau, Bonnet, Leschziner, & Menter, 2002). The dimensions of the squared-back Ahmed body are defined as follows: the height (H) is 1, the width (W) is 1.37H, the length (L) is 3.36H, and the round edges at the front of the body is 0.35H. The size of the fluid domain must be sufficiently large to observe near-wake flow structures behind the squared-back Ahmed body. There are 6.3L in length, 1.6L in width, 2L in height, and an inlet length is 1.3L. The clearance between the body and the ground is 0.1769H as shown in figure 1 and figure 2. Continuously blowing jets are placed at the top of the rear part of the body with a width of 0.05H and a length of 1.37H.

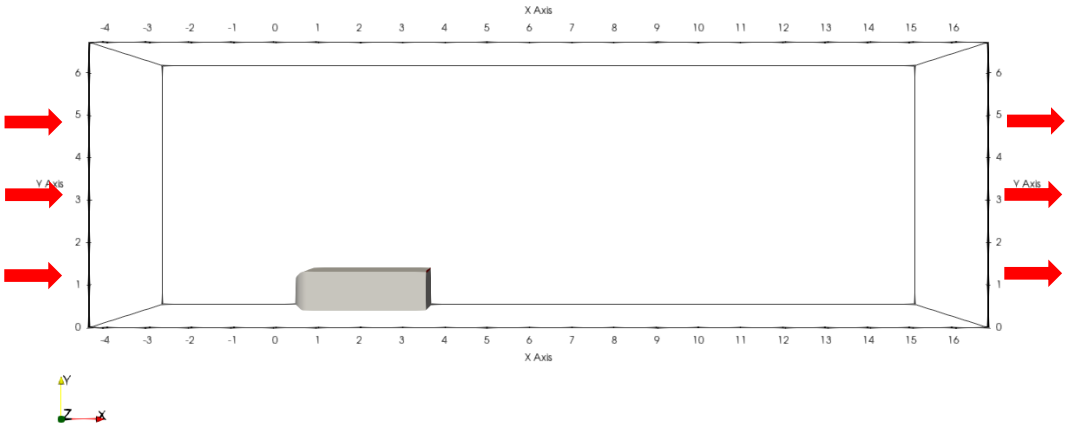

Figure 1: Computational domain.

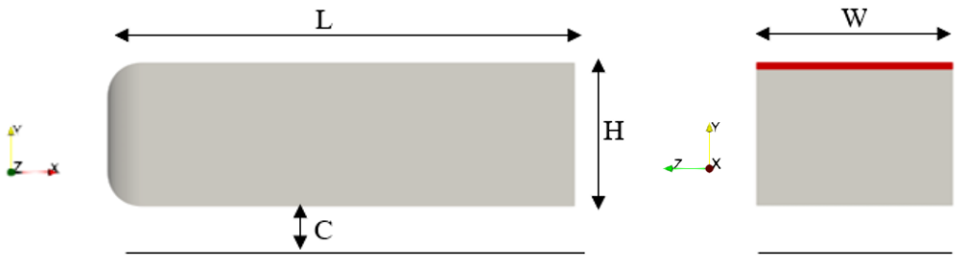

Figure 2: Drawing of squared-back Ahmed body and jet actuator (red).

Part 2: Define The Boundary Conditions, Properties Of Fluid, And Parameters

The viscous incompressible flow in Newtonian fluid is studied. Fluid flows around the squared-back Ahmed body at Re_H = 33,000 are investigated and compared to the literature (Evstafyeva, 2018). Steady-state simulations are considered. Kinematic viscosity of fluid is 1.5×10^{-5} m^2/s and reference pressure p_∞ is zero Pascal, respectively. The boundary conditions applied to all controlled and uncontrolled simulation cases are defined as follows: a constant velocity at the inlet is

0.495 m/s in the x- direction (the streamwise direction), no-slip boundary conditions are applied to the ground and the body surfaces, pressure at the outlet is set to zero, free-slip boundary conditions are applied to all sides of the domain. For uncontrolled flow, the no-slip boundary condition is applied at the rear part of the body as usual. For controlled flow, on the other hand, continuously blowing jets are placed at the top of the rear part of the body by defining the magnitude of the jet velocity, while the no-slip boundary condition is applied to the others. It is noted that six different cases for controlled flow are investigated based on the magnitude of the jet velocity at 20%, 40%, 50%, 60%, 80%, and 100% of the free-stream velocity, U_∞, respectively.

Part 3: Generate a mesh of the fluid domain

In the computational domain, there are approximately 16.25 million nodes and 15.63 million cell elements which are sufficient for the simulation analysis. Mesh resolution was validated by the method of mesh convergence. Therefore, the result of the simulation is not significantly changing when increasing the mesh resolution with the previous one. Hexagonal meshes are mainly utilized. Mesh qualities are examined by non-orthogonality and skewness. The mean value of the non-orthogonality is 4.42. It is noted that the numerical treatment is needed if the value of the non-orthogonality is greater than 75. The maximum skewness is 2.48, where the value between 0 and 4 is good and acceptable (Greenshields, 2018; Jasak, 1996). The first layer thickness of the mesh is measured by y+. Where y+ is dimensionless wall-normal distance. The maximum and average values of the first y+ on the surface of the body are 1.033 and 0.0128. Therefore, these layers can capture the phenomena of the fluid at the near wall as well.

Part 4: Perform the simulations and investigate the results

Computational fluid dynamics (CFD) is employed to investigate the physical phenomena of the flow around the squared-back Ahmed body using numerical methods based on the incompressible Navier-stokes equations. The Reynolds-averaged Navier–Stokes (RANS) equations are utilised in the present study. The momentum and continuity equations are presented in equation (1) and (2), respectively.

$$\frac{D\bar{u}_i}{Dt} = \frac{\partial \bar{p}}{\partial x_j} + \nu \frac{\partial^2 \bar{u}_i}{\partial x_j \partial x_j} - \frac{\partial \tau_{ij}}{\partial x_j} \tag{1}$$

$$\frac{\partial \bar{u}_i}{\partial x_i} = 0 \tag{2}$$

, where τ_{ij} are the nonlinear Reynolds stress terms. Thus, the Boussinesq hypothesis is introduced to solve the RANS equations by redefining the Reynold stress terms as follows:

$$\tau_{ij} = -\rho\overline{u'v'} = \mu_t \left(\frac{\partial \bar{u}_j}{\partial x_i} + \frac{\partial \bar{u}_i}{\partial x_j} \right) \tag{3}$$

The k-ω SST turbulence model is widely used for simulation in the aerodynamics field and is suitable for analyzing flow separation which involved adverse pressure gradients (Banjan, & Raikar, 2021; Peng, Eliasson, & Davidson, 2007). The dynamic eddy viscosity μ_t is modeled by the k-ω SST turbulence model. The two transport equations, turbulent kinetic energy, and specific dissipation rate, are presented in equations (4) and (5), respectively. In the two-equation eddy-viscosity (k-ω SST)

turbulence model, all the constants are defined according to the standard model (Menter & Esch, 2001; Menter, 2009), whereas the eddy viscosity is redefined by the shear-stress transport model.

$$\frac{D\rho k}{Dt} = \tau_{ij}\frac{\partial \bar{u}_i}{\partial x_j} - \beta^* \rho k + \frac{\partial}{\partial x_j}\left[(\mu + \sigma_k \mu_t)\frac{\partial k}{\partial x_j}\right] \quad (4)$$

$$\frac{D\rho\omega}{Dt} = \frac{\gamma}{\nu_t}\left(\tau_{ij}\frac{\partial \bar{u}_i}{\partial x_j}\right) - \rho\beta\omega^2 + \frac{\partial}{\partial x_j}\left[(\mu + \sigma_\omega \mu_t)\frac{\partial \omega}{\partial x_j}\right] + 2\rho\sigma_{\omega 2}(1 - F_1)\left(\frac{1}{\omega}\frac{\partial k}{\partial x_j}\frac{\partial \omega}{\partial x_j}\right) \quad (5)$$

Investigation the result of simulation by considering the pressure field, velocity field, force and moment coefficients, characteristic of wake and pressure recovery. This study, simulation results for the uncontrolled case at Re_H = 33,000 are compared to the literature (Evstafyeva, 2018) as shown in table 1. The drag coefficient C_d and the recirculation length are assessed. It shows that the drag coefficient, C_d, obtained from the simulations agrees well with the results obtained from the literature. The recirculation length is slightly different. RANS simulations produce longer recirculation length than LES simulations.

Table 1: Uncontrolled flow around the squared-back Ahmed body at Re_H = 33,000.

Model	Number of Nodes		C_d	Recirculation Length
	Overall	Body		
k – ω SST (simulation)	≈ 16.3 million	456,572	0.3177	1.96H
LES from (Evstafyeva, 2018)	≈ 86.5 million	524,288	0.3180	1.50H

After validation the result to the literature with uncontrolled flow. In case of controlled flow, performed the simulation according to the parameters in Part 2.

Results

Flow visualization of fluid flow around the squared-back Ahmed body have interesting regions all around the object. For the front of an object, the front point collides with the fluid is a point of low velocity and high pressure, this point is called the stagnation point. As the fluid flows through the arc of the object, the pressure begins to decrease and the velocity increases until the fluid's pressure begins to drop again. The fluid will escape from the surface of the object. At this point is called separation point. In the figure 3 (a), there are two separation points on the upper and lower on the front part. For the flow separation layer, the upper region larger than the lower region. Fluid behind the body has a low velocity and low pressure, this region is called wake region. Inside of wake region, at the back of the body found the recirculation of streamline as shown in the figure 3 (c).

Force and moment coefficients and the recirculation length obtained from both uncontrolled and controlled cases with different jet velocities are presented in table 2. It shows that the drag coefficient is relatively large compared to other coefficients. This implies that the drag force is the most dominant force acting on the body due to pressure difference between the front and the rear part of the body. The optimum drag coefficient C_d can be achieved when the continuously blowing jet velocity is approximately equal to $0.6U_\infty$. The magnitude of negative lift coefficient is maximum in uncontrolled flow and decreased when the flow controlled increased. The side force coefficient and moment coefficients in roll/pitch/yaw- axes are relatively low, less than 0.01.

Table 2: Force and moment coefficients and the recirculation length from both uncontrolled and controlled cases with different jet velocities.

Jet Velocity (U_{jet}/U_{∞})	C_d	C_s (10^{-4})	C_l	$C_{m,roll}$ (10^{-6})	$C_{m,pitch}$	$C_{m,yaw}$ (10^{-5})	Recirculation Length
Uncontrolled	0.3177	1.4190	-0.1605	-2.4667	-0.0148	1.0132	1.96H
0.2	0.3109	0.0665	-0.1575	-0.8404	-0.0133	-1.0721	2.02H
0.4	0.3079	0.3052	-0.1502	-1.1161	-0.0126	-8.3246	2.04H
0.5	0.3063	-0.4045	-0.1467	0.0350	0.0103	-1.5994	2.05H
0.6	0.3056	-0.0584	-0.1429	-0.9171	0.0092	-1.3374	2.04H
0.8	0.3086	0.1146	-0.1365	-0.8140	0.0073	-1.0557	1.95H
1.0	0.3205	-1.4791	-0.1352	2.2932	0.0064	-2.8371	1.88H

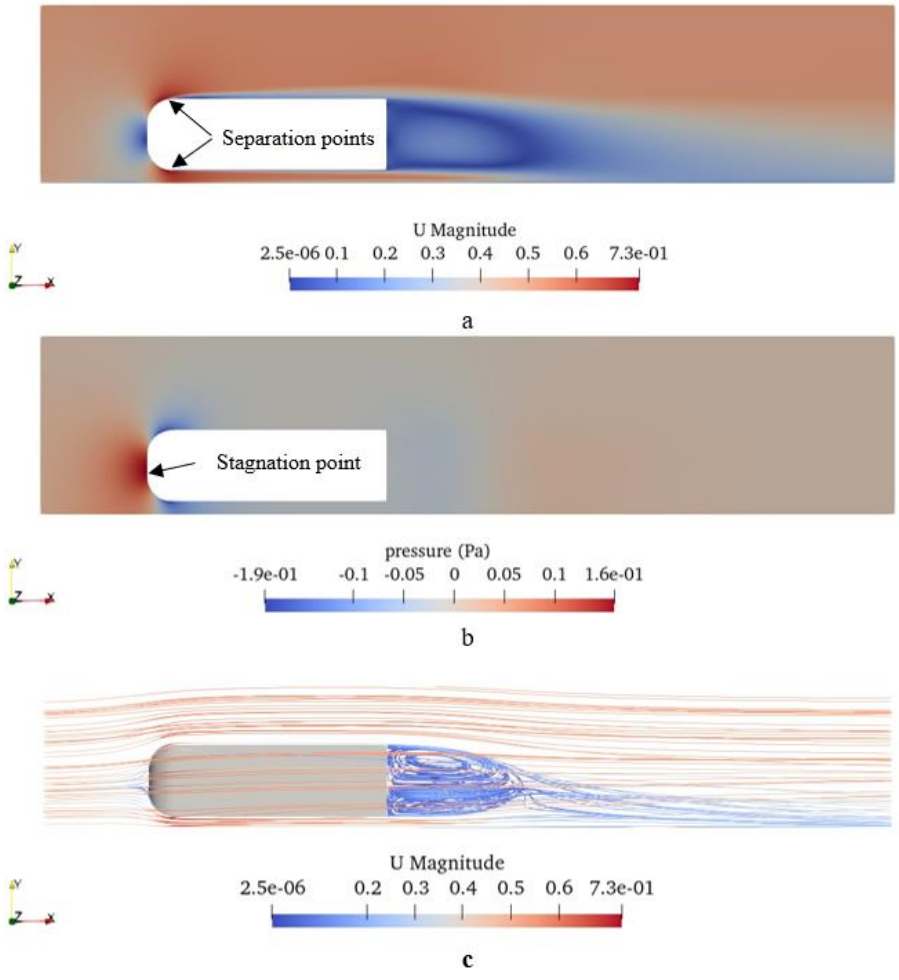

Figure 3: Flow visualizations of fluid around the bluff body, (a) velocity, (b)pressure and (c) streamline.

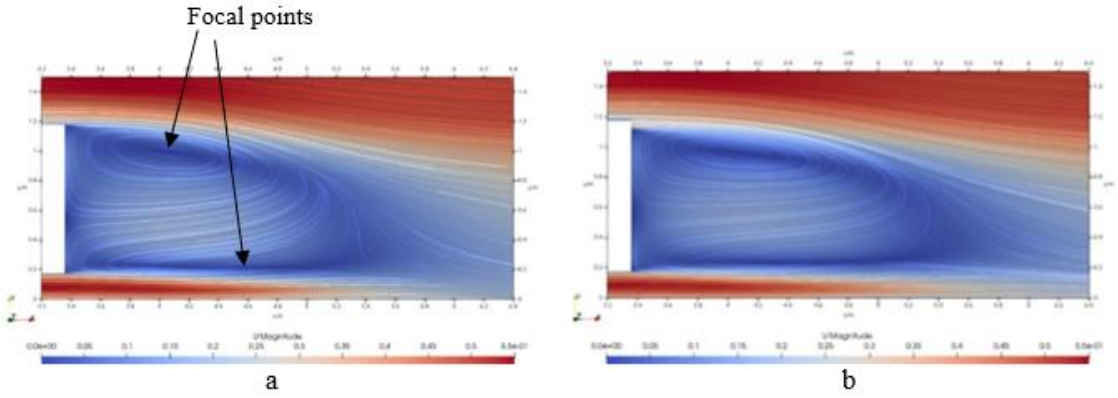

Figure 4: Comparison of the streamwise velocity field and the streamline of downstream of the squared-back Ahmed body at Re_H = 33,000 on the centreline plane: a) Uncontrolled flow, (b) Controlled flow with U_{jet}/U_∞ = 0.6.

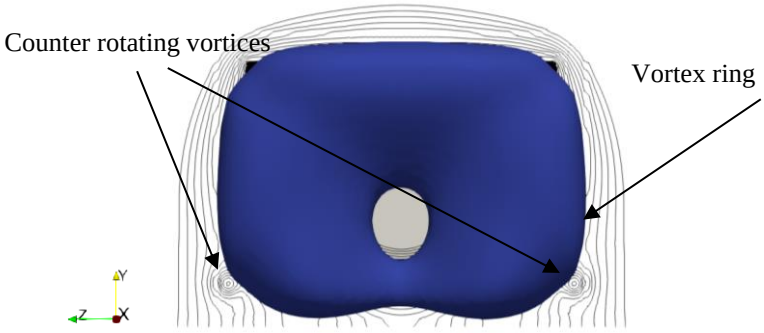

Figure 5: Vortex ring and counter rotating vortices detected by an isosurface of the pressure p = -0.0306 m^2s^{-2} with a pressure contour on the plane x = 3.36H.

After this section will be focused on behind the body because fluid at front part of uncontrolled and controlled flow are very similar. For uncontrolled flow, figure 4(a) reveals that boundary-layer separation occurs at the sharp edge of the rear part of the body due to extremely high adverse pressure gradient. There are two recirculation regions forming behind the rear part of the body, primary and secondary recirculation regions. Both recirculation regions are not symmetry along the centreline plane as a result of the ground effect and they also circulate in the opposite direction. The length of the recirculation zone is 1.96H. The magnitude of velocity in the recirculation zones is relatively small; these recirculation zones are so-called dead zones. Two critical points appear in the recirculation region, and they are defined as focal points. The vortex ring and counter rotating vortices are formed at the back of the body as shown in figure 5.

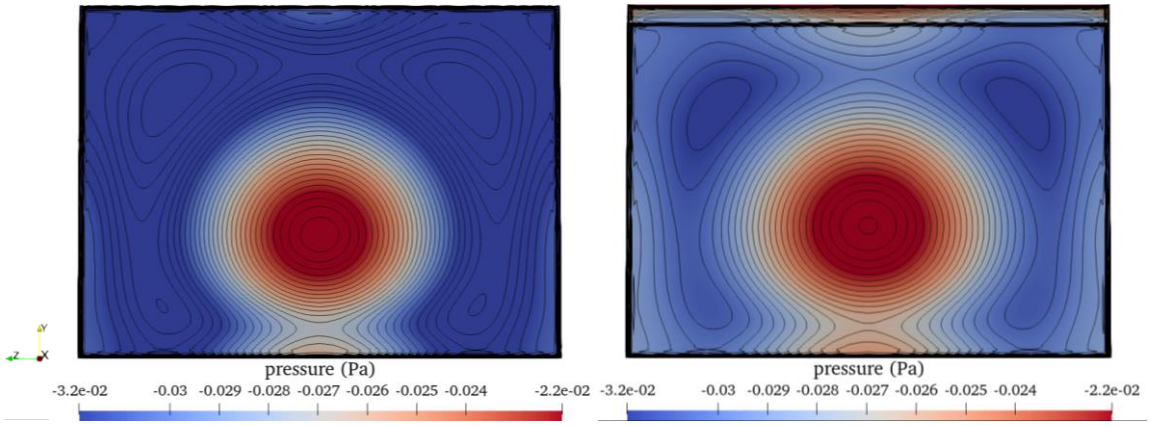

Figure 6: Pressure distribution and contour at the rear end of the body at Re_H = 33,000: (a) uncontrolled flow, (b) controlled flow with U_{jet}/U_∞= 0.6.

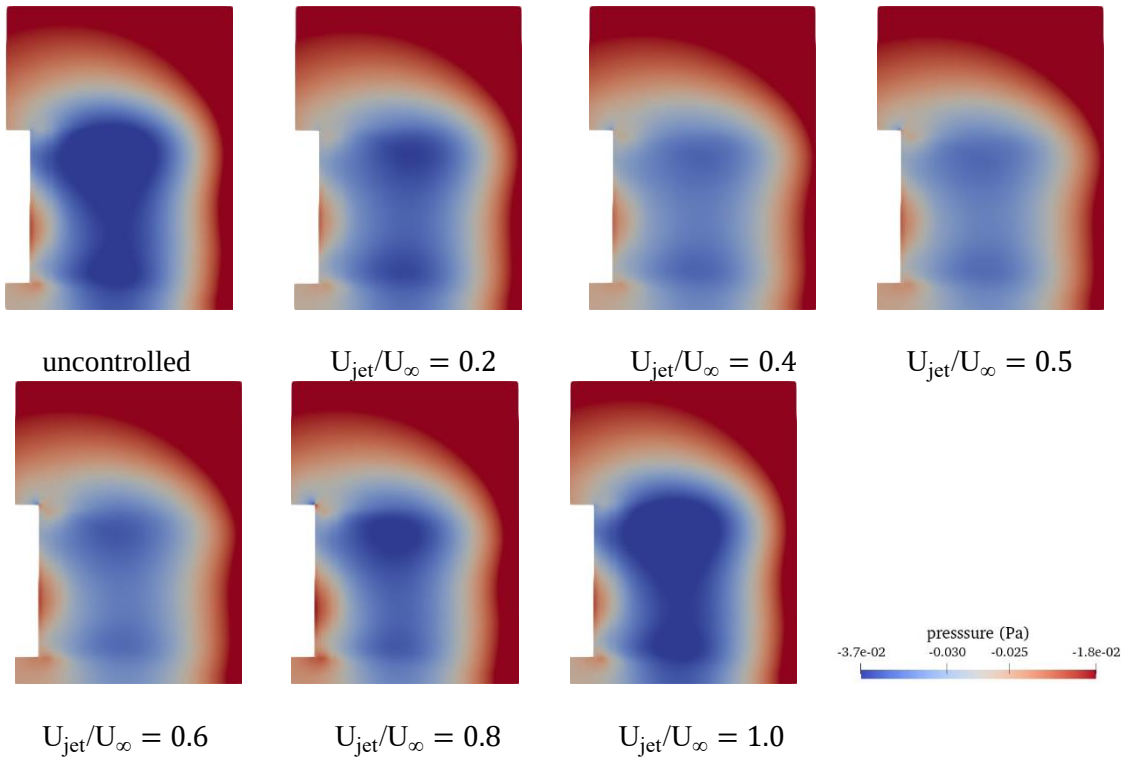

Figure 7: Pressure field behind the body at Re_H = 33,000 for uncontrolled and controlled flow.

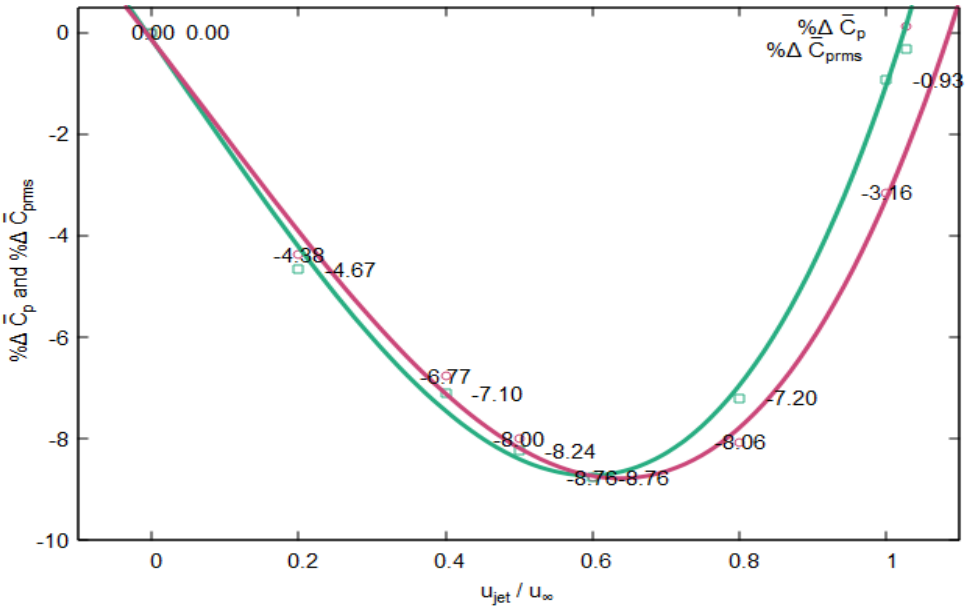

Figure 8: Percentage change of average base pressure coefficient and root-mean-square base pressure coefficient at different jet velocities.

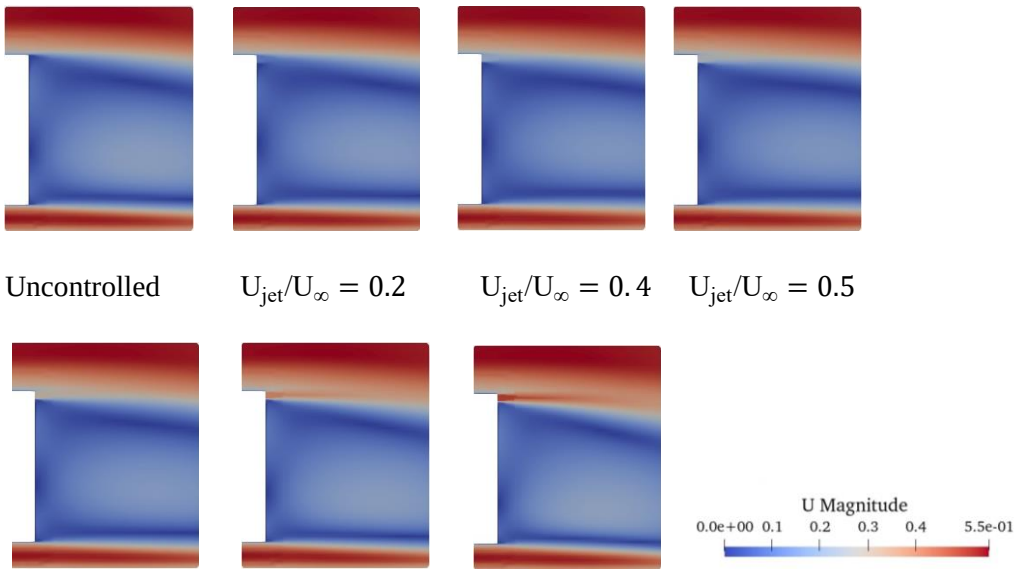

Figure 9: Velocity distribution at the back of the body for uncontrolled and controlled flow.

Figure 6 shows that continuously blowing jets installed at the top of the rear part of the body can recover the base pressure. For the high pressure at the middle of rear part is also called dead zone. The shape of vortex ring can also represeneted by the low pressure (blue area) as shown in the figure 7, the upper part or vortex ring lager than the lower part. Overview of pressure in wake region trend to increase along to the velocity of controlled flow. Until $U_{jet}/U_{\infty} = 0.6$, pressure vary inversly with the jet velocity. The percentage change of average base pressure coefficient $\overline{C}_p$ and root-mean-square base pressure coefficient $\overline{C}_{prms}$ at different jet velocities are presented in figure 8. When the jet

velocity is gradually increased from U_{jet}/U_{∞} = 0.0 to U_{jet}/U_{∞} = 0.6, the mean base pressure is moderately recovered. At U_{jet}/U_{∞} = 0.6, the optimum base pressure recovery of 8.76% is achieved, corresponding to 3.81% in drag reduction. The result also shows that the recirculation length is 2.04H. When the value of U_{jet}/U_{∞} is greater than 0.6, the mean base pressure recovery becomes worse. The flow also observed that the fluid is separated the layer as shown in the Figure 9.

Discussion

The side force coefficient is low may be caused by the body are symmetry in centreline and distance between the side of the body far enough for neglected effect from the wall of fluid domain. The moment coefficients are very low. It can be argued that the body have a relatively symmetrical shape and pressure difference around the body is small causes the moment almost completely cancelled.

The negative lift coefficient is obtained from pressure difference between the topside and the underside of the body due to the ground effect. The ground effect occurs when the fluid flows through the underside of the body. The flow cross-section area decreases, thereby accelerating the flow and reducing the pressure of the fluid. In consequence, the downforce (negative lift force) is generated. In addition, the acceleration effect of the fluid causes flow separation layer at both upper and lower of front area of the body. However, separation layer of upper region lager than lower region also may be caused by the ground effect.

This study focused on the form drag which the one of reason affect to the drag coefficient. Try to improve the pressure behind the body by using the continuously blowing jet. Adding tangential momentum by means of continuously blowing jets results in the modification of the base pressure. The suitable of jet velocity is significantly for drag reduction. For U_{jet}/U_{∞} less than or equal to 0.6 can reduce the drag coefficient as well. It is suggested that continuously blowing jets lessen pressure gradient behind the body by transferring momentum to the recirculation zones. Consequently, the recirculation length becomes longer. Until $U_{jet}/U_{\infty} = 0.6$,this case is the most reduce drag coefficient and the best base pressure recovery. It is suggested that the cross-section area of the bubble separation zone is decreased and elongated compared to the uncontrolled case as shown in figure 4(b). For U_{jet}/U_{∞} greater than 0.6. Although it can reduce the drag and improve base pressure, but it not related in the same direction as the jet velocity increase. May be waste of resources more than necessary. This might be due to the jet blockage effect as shown in figure 8. It is suggested that the separated shear layer generated from the sharp edge of the rear part of the body inhibits the elongation of the wake region. In consequence, less momentum transfer causes a decrease in the recirculation length.

In the engineering design of the lorry, a square hole is drilled at the top of the rear part of the lorry and the jet actuator is mounted. In this design, there is no need to modify the exterior of the lorry that may affects its loading capacity, but the size of square hole and power of jet actuator should be chosen appropriate for each situation.

Conclusion

Numerical simulations of incompressible flow over the squared-back Ahmed body, representing a generic lorry model, are performed at Re_H = 33,000. The Reynolds-averaged Navier–Stokes (RANS) equations with the $k-\omega$ SST turbulence model are employed. Continuously blowing jets are installed at the top of the rear part of the squared-back Ahmed body to alter the wake structures behind it. Six different cases are investigated based on the magnitude of the jet velocity at 20%, 40%, 50%, 60%, 80%, and 100% of the free-stream velocity, U_{∞}, respectively. The result shows

that the optimum drag coefficient C_d can be achieved when the continuously blowing jet velocity is approximately equal to $0.6U_\infty$, corresponding to 3.81% in drag reduction. Physical characteristics of the near-wake flow is also carried out. Recirculation zones, vortex ring, and counter rotating vortices can be observed. It is likely that continuously blowing jets alter the momentum transfer in the recirculation zones, affecting the geometry and shape of the wake. In consequence, the mean base pressure is recovered resulting in drag reduction.

References

Ahmed, S. R., Ramm, G., & Faltin, G. (1984). Some salient features of the time-averaged ground vehicle wake. *SAE Transactions*, *93*(2), 473-503.

Banjan, V., & Raikar, D. (2021). Design Analysis and Shape Optimization of Cabin to reduce Aerodynamic Drag in a Semi-Truck by using Computational Fluid Dynamics. *International Research Journal of Engineering and Technology (IRJET)*, *8*(11), 478-492.

Barros, D., Borée, J., Noack, B. R., Spohn, A., & Ruiz, T. (2016). Bluff body drag manipulation using pulsed jets and Coanda effect. *Journal of Fluid Mechanics*, *805*, 422-459.

Bradley, R. (2000). *Technology Roadmap for the 21st Century Truck Program: A Government Industry Research Partnership.* Washington, DC, USA: USDOE Office of Heavy Vehicle Technologies.

Clapperton Surfleet, Ben Lewis. (2017). *Drag reduction of bluff bodies by passive control of boundary layer transition and separation.* Doctoral dissertation, Imperial College London. London, UK.

Evstafyeva, O. (2018). *Simulation and feedback control of simplified vehicle flows.* Ph.D. dissertation, Imperial College London. London, UK.

Gad-el-Hak, M. (2000). *Flow Control: Passive, Active, and Reactive Flow Management*. Cambridge University Press. UK.

Gerrard, J. H. (1966). The mechanics of the formation region of vortices behind bluff bodies. *Journal of fluid mechanics*, *25*(2), 401-413.

Grandemange, M., Cadot, O., & Gohlke, M. (2012). Reflectional symmetry breaking of the separated flow over three-dimensional bluff bodies. *Physical review E*, *86*(3), 035302.

Greenshields, C. J. (2018). OpenFOAM-The OpenFOAM Foundation-User Guide.

IPCC. (2014). *Climate Change 2014: Mitigation of Climate Change. Contribution of Working Group III to the Fifth Assessment Report of the Intergovernmental Panel on Climate Change.* Cambridge University Press, Cambridge, United Kingdom and New York, USA.

Jasak, H. (1996). *Error analysis and estimation for the finite volume method with applications to fluid flows*. Ph.D. Thesis, Imperial College London.

Manceau, R., Bonnet, J. P., Leschziner, M., & Menter, F. (2002). Proc. 10th ERCOFTAC (SIG-15)/IAHR/QNET-CFD Workshop on Refined Turbulence Modelling.

Menter, F. R. (2009). Review of the shear-stress transport turbulence model experience from an industrial perspective. *International journal of computational fluid dynamics*, *23*(4), 305-316.

Menter, F., & Esch, T. (2001). Elements of industrial heat transfer predictions. In *16th Brazilian Congress of Mechanical Engineering (COBEM)* (Vol. 20, pp. 117-127). Minas Gerais, Brazill.

Peng, S. H., Eliasson, P., & Davidson, L. (2007). Examination of the shear stress transport assumption with a low-Reynolds number k-omega model for aerodynamic flows. *In 37th AIAA Fluid Dynamics Conference and Exhibit (p. 3864).* Miami, Florida: AIAA.

Roshko, A. (1955). On the wake and drag of bluff bodies. *Journal of the Aeronautical Sciences*, *22*(2), 124-132.

COMPARISON OF THE CLASSIFICATION OF PHONOCARDIOGRAMS WITH BREATHING SOUND NOISE BY MACHINE LEARNING ALGORITHMS

Neungreutai Prasert[1], Thanaset Thosdeekoraphat[2], and Jessada Tanthanuch[3*]

[1]School of Biomedical Innovation Engineering, Suranaree University of Technology, Thailand
[2] School of Electronic Engineering, Suranaree University of Technology, Thailand
[3] School of Mathematics, Suranaree University of Technology, Thailand
***Corresponding author, E-mail:** jessada@g.sut.ac.th

Abstract

This research aims to classify between normal heart sounds and abnormal heart sounds (heart murmurs and clicks) by machine learning techniques. This study made the assumption that the obtained heart sound may be interfered with by the breath sound noise. The test files were manipulated by overlaying the breathing sound noise on the phonocardiograms of heart sounds. The data of breathing sound noise and heart sound was obtained from Respiratory Auscultation (https://www.mediscuss.org/respiratory-auscultation/) and Heart Sound & Murmur Library, University of Michigan, respectively. Moreover, the files of heart sounds were processed by changing tempos to be faster from 0%, 10%, 20%, 30%, 40%, and 50%, which were done by Audacity software. The different tempos of each heart sound file represent the different heartbeat rates of the same person. In this work, five techniques of machine learning algorithm, which were Random Forest, Neural Network, Deep Learning, Support Vector Machine, Naïve Bayes, were applied for making the model of classification. The methods used for model validation were split validation and cross-validation. The data for classification were the images of the waveform of processed noisy heart sounds and spectrogram of the processed sound. Software used for the working of classification was RapidMiner studio. It was found that the Random Forest technique with cross-validation of a spectrogram of sound files provided the best performance, which had accuracy = 93.69%, precision = 97.41%, recall = 89.68%, and F1-score = 93.39%.

Keywords: Phonocardiogram Spectrogram Classification Spectrogram Machine Learning

Introduction

According to the World Health Organization, cardiovascular diseases (CVDs) are one of the main causes of death globally. An estimated 17.9 million people died from CVDs in 2019 representing 32% of all global deaths. Out of the 17 million premature deaths (under the age of 70) due to noncommunicable diseases in 2019, 38% were caused by CVDs. It is important to detect cardiovascular disease as early as possible so that management with counseling and medicines can begin (WHO, 2021). Auscultation by using a stethoscope for listening to the heart sound is a part of physical examination. The stethoscope is a basic medical device that doctors always use to listen to mechanical valvular activity. It is a valuable method for CVDs detection. These diseases could be identified easily with the variations in the sound produced due to heart activity. That is the most primary diagnosis method for the initial detection of heart valves which is also an economical and simple screening test.

Heart sounds are created by blood flow and vibrations of tissues during the cardiac cycle. Under normal conditions, blood flow is laminar and silent. With structural or hemodynamic changes

turbulent flow results, which causes vibrational waves. These waves are transmitted through the chest wall that is translated into sounds known as heart sounds or Phonocardiogram "PCG". PCG signal analysis is a common method for evaluating the condition of the heart and detecting possible anomalies.

Artificial intelligence (AI) is a science that gathers knowledge in many disciplines. In particular, it is the combination of science and engineering to develop machines or computer systems to be intelligent, able to think, calculate, analyze, learn and make decisions as rational as the human brain, and be able to learn, develop and improve its work processes to increase the potential of artificial intelligence itself (Sittichanbuncha, 2021). AI has been developed since the 1950s to the present day and can be used in a variety of areas, including the medical fields and healthcare industry such as diagnosing diseases detecting lung cancer, classifying skin lesions in skin images assessing the risk of sudden cardiac death or other heart diseases based on electrocardiograms, cardiac MRI images, and including phonocardiogram (Schmitt, 2020). Currently, Artificial intelligence (AI) algorithms are widely used in the classification of heart sound abnormalities due to the analysis of heart sound signals playing an irreplaceable role in the early diagnosis of heart disease and containing a large amount of pathological information about each part of the human heart. Heart sounds can be detected and recorded by Phonocardiogram (PCG) (Yang et al., 2019). As a non-invasive method to detect and diagnose heart disease, PCG signals have been paid more and more attention by researchers.

Research Objectives

1. To classification normal heart sound and abnormal heart sound from obtained phonocardiogram with breathing sound noise fil es by machine learning algorithms.
2. To compare the performance of 5 machine learning algorithms in the classification.

Literature Review

Aktar, and Andrei (2020) proposed a heartbeat audio classifier software design that could differentiate normal heartbeats and heart murmurs by Convolutional Neural Network (CNN) algorithm. The software could also differentiate the types of heart sounds. The CNN achieved an accuracy of approximately 79% on unseen test data, with an AUROC score of 0.78.

Baydoun, Safatly, Ghaziri, and El Hajj (2020) proposed an approach to combine multiple classification models of heart sounds to improve accuracy. The classification system by combining the LogitBoost model and the Bagging model provided the best score of 86.6% of accuracy, with a sensitivity and specificity of more than 90%, and 83% respectively.

Bourouhou, Jilbab, Nacir, and Hammouch (2020) proposed a classification algorithm based on the extraction of 20 features from segmented phonocardiogram (PCG) by applying four types of machine learning classifiers, which were k-nearest neighbor (KNN), support vector machines (SVM), Tree Classifier, and Naïve Bayes. The results showed that Naive Bayes had the best classification performance.

Zhang, Han, and Deng (2019) proposed the method for heart sound detection using the temporal quasi-periodic features of the heart sound signals. The analysis was done by AMDF of the heart sound spectrogram and the short-term and long-term dependency relation within the temporal quasi-periodic features extracted by long short-term memory (LSTM). This method could effectively detect abnormal heart sound.

Chowdhury, Khandakar, Alzoubi, Mansoor, Tahir, Reaz, and Al-Emadi (2019) proposed the prototype model of a smart digital-stethoscope system to monitor a patient’s heart sounds. It helped in

diagnosis any abnormality in a real-time manner. The model was designed by modifying an analog stethoscope. The stethoscope was added up by a miniaturized microcontroller with built-in Bluetooth low energy for digitization and transmission. The obtained data were classified by machine learning algorithms, which were Decision tree, discriminant analysis, support vector machines (SVM), k-nearest neighbor (KNN), and ensembles classifiers. The results showed that the Ensemble algorithm could outperform all the trained competition algorithms with an overall accuracy of 86.02%.

Yang, Li, Zhang, and Yang (2020) proposed the novel envelope extraction model which could use to estimate the cardiac cycle of each PCG signal. They combined the empirical mode decomposition (EMD) technique and the proposed envelope model to extract the time-domain features. The feature vectors were extracted from both the frequency-domain features and wavelet-domain features. By using the support vector machine (SVM) classifier to detect the normal and abnormal PCG signals, the model had an accuracy of more than 96%.

Methodology

1. The heart sound files

The PCG of heart sound files were obtained from Heart Sound & Murmur Library, University of Michigan. They were MP3-type with a 128kbps bit rate. There were 2 files of normal heart sounds and 21 files of abnormal heart sound including murmurs and clicks sounds.

2. Breathing sound noise preparation

The breathing sound noise was obtained from Respiratory Auscultation (https://www.mediscuss.org/respiratory-auscultation/). The file was also MP3 type with a 192kpbs bit rate. The sound was extended by repeating the sound to be longer closed to the time duration of heart sound by Audacity software.

3. Overlaying breathing sound noise over heart sound

In this step, we overlaid the extended breathing sound and heart sound files together by the Audacity software.

4. Changing tempo

We considered that the different activities of each person change the speed of breathing rate and heart rate. To simulate the situation, we made up the data by changing the tempos of the noisy heart sounds by Audacity software. The sound files were changed by setting the tempo to be faster from 0%, 10%, 20%, 30%, 40%, and 50%, and then exported to WAV files format. This technique still preserved the frequency of the wave.

5. Conversion to PNG spectrogram

Even the classification software, RapidMiner studio, had no audio library for classification, but it has many powerful functions for image processing. In this step, we wanted to make a comparison of using waveform files and spectrogram of sound as data sources for the machine learning part. Audacity software could display spectrogram in the Mel-frequency scale of each WAV file. The PNG files of the spectrogram were exported for classification.

6. Setting the machine learning system for classification between normal heart sound and abnormal heart sound

In the last step, we set RapidMiner studio software to classify normal and abnormal heart sound. We used split validation and cross-validation for data manipulation. Here, 5 techniques of machine learning algorithm, which were Random Forest, Neural Net, Deep Learning, Support Vector Machine, Naïve Bayes, were applied for making the model of classification. The proposed 5 methods are very well-known machine learning techniques using in the classification. For the model obtained, we considered the confusion matrices and calculated accuracy, precision, recall, and F1-score.

Results

1. The heart sound files

We provided examples of the time waveform of a PCG cardiac cycle in figure 1.

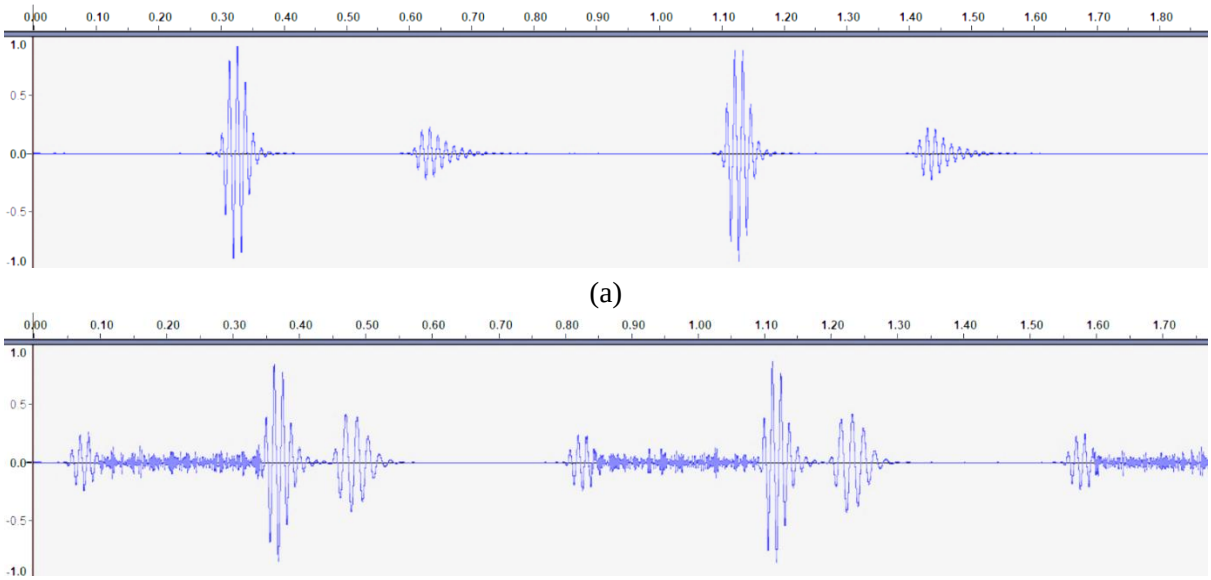

(a)

(b)

Figure 1: The time waveform of a PCG cardiac cycle in (a) normal and (b) abnormal

2. Breathing sound noise preparation

By the original breathing sound (figure 2 (a)), we extended the sound noise by repeating the sound (figure 2 (b)).

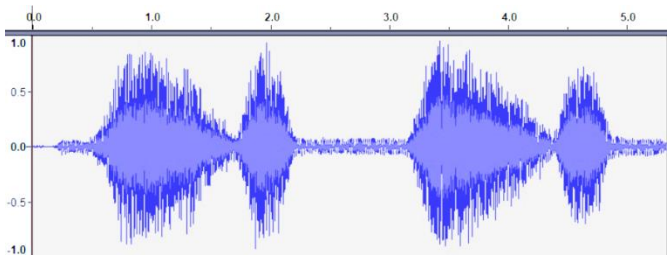

(a)

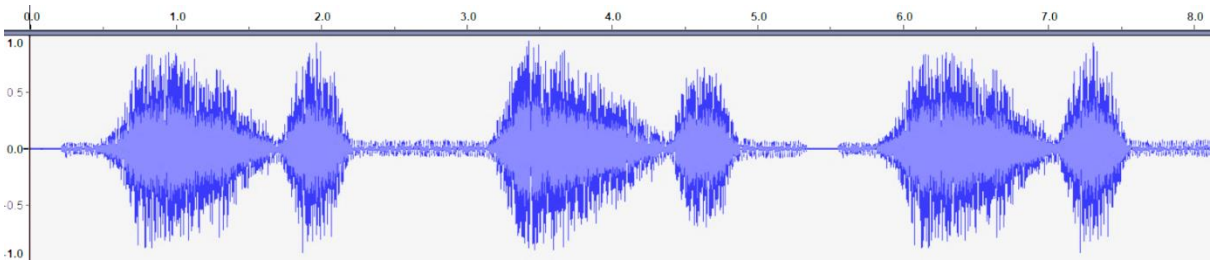

(b)

Figure 2: (a) Original breathing sound noise, and (b) extended sound noise

3. Overlaying breathing sound noise over heart sound

The PCG sound and extended breathing sound (figure 3 (a)) were combined by overlaying (figure 3 (b))

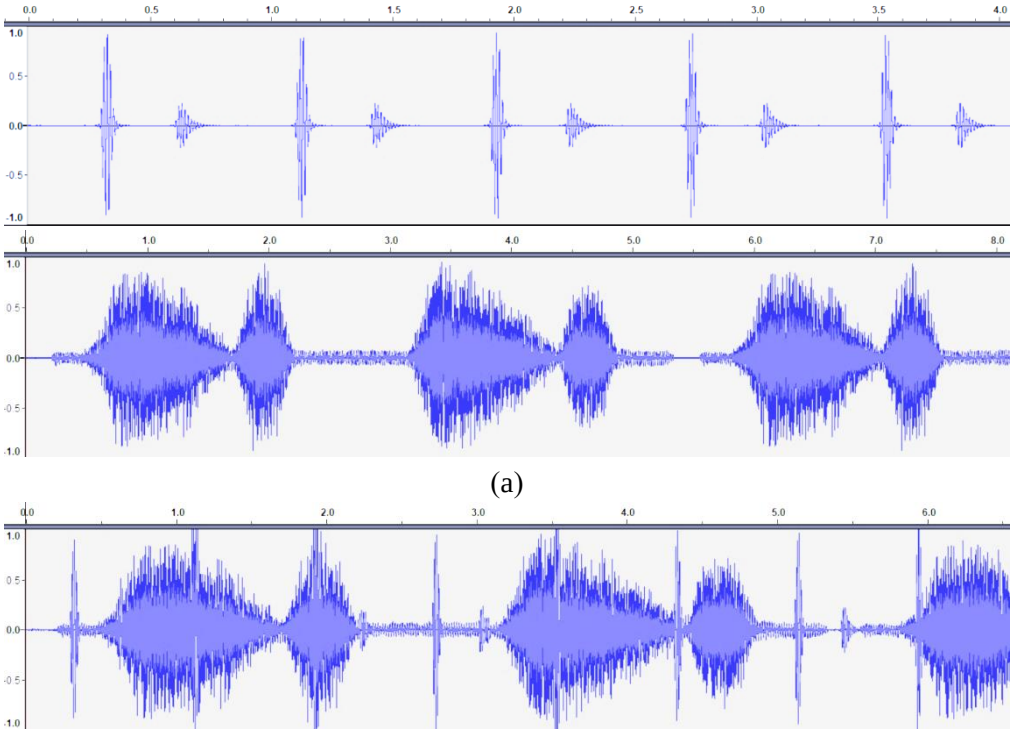

(a)

(b)

Figure 3: Combining PCG sound and extended breathing sound (a) and results (b)

4. Changing tempo

The results of changing tempos were presented in figure 4.

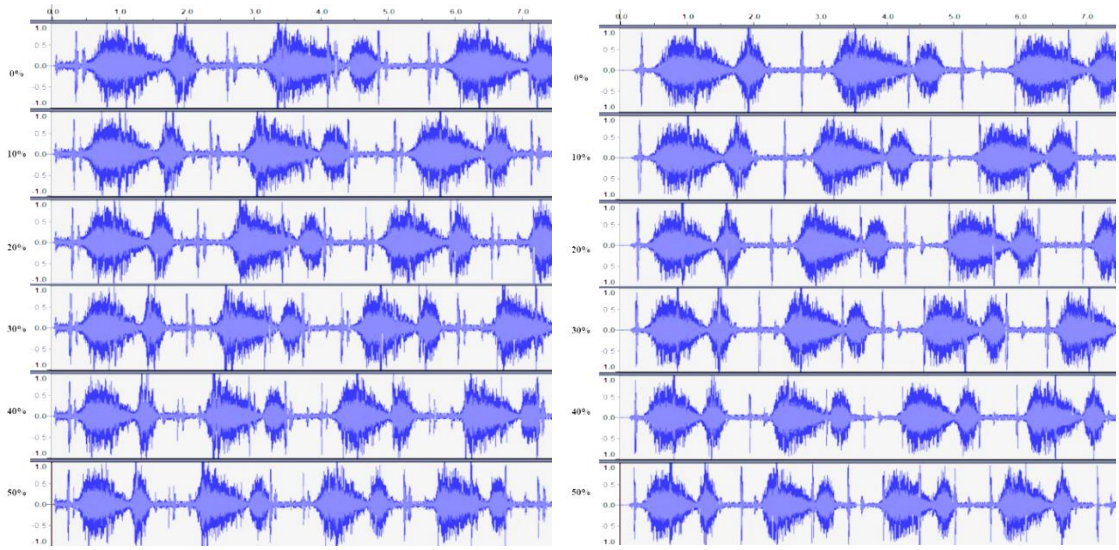

(a) (b)

Figure 4: Examples of PCG sound modified by changing tempos
(a) normal heart sound (b) abnormal heart sound

5. Conversion to PNG spectrogram (spectrogram in Mel-frequency scale)

By Audacity software, spectrogram in Mel-frequency scale of each WAV was created and exported as PNG files.

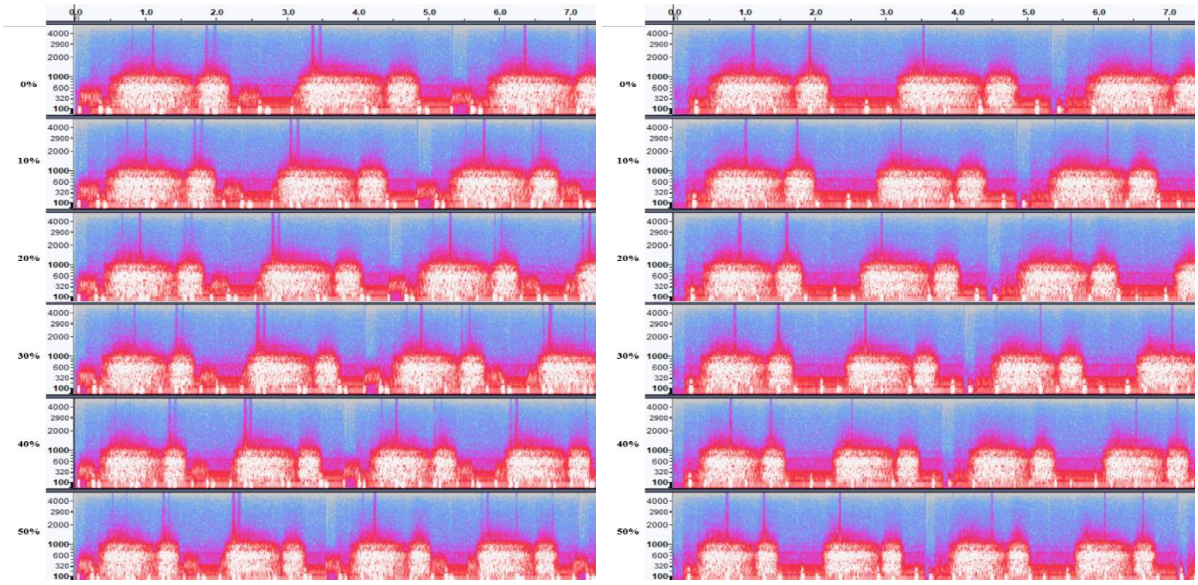

(a) (b)

Figure 5: Examples of a spectrogram of noisy PCG heart sound
(a) normal heart sound (b) abnormal heart sound

6. Setting the machine learning system for classification between normal heart sound and abnormal heart sound

RapidMiner Studio is a software that can do coding a program by block diagrams. For setting the machine learning system, we did programming as the following steps.

6.1 Prepare Datasets

The waveform and spectrogram images were separated into 2 groups, normal and abnormal. The data would be used for training and testing the models. The block diagram code and the setting were shown in figure 6. The data used as input data were waveform images and spectrogram images.

Figure 6: Block diagram for datasets preparation

6.2 SMOTE Up-sampling

Since the ratio of a number of normal heart sound data (12 files) and abnormal heart sound data (126 files) were quite different. For reducing the unbalance data problem, we applied Synthetic Minority Over-sampling Technique or SMOTE to up-sampling the number of normal heart sound data.

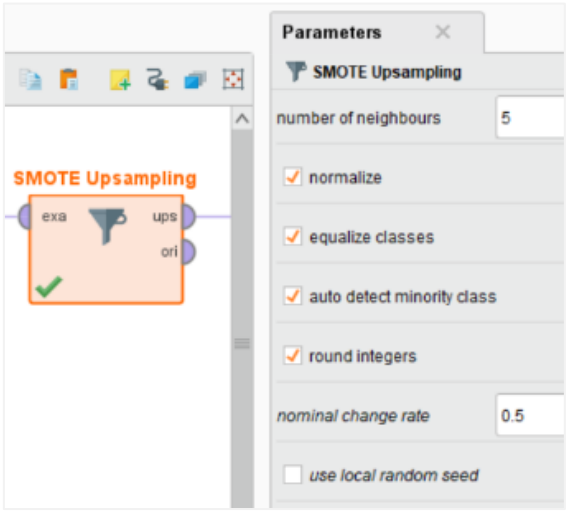

Figure 7: Block diagram for SMOTE up-sampling setting

6.3 Process

We used the “Multiply” operator for creating copies of our data. The Multiply operator helped us in making many machine learning techniques models according to our suggested algorithms parallelly. Here, the multiply” operator was connected to Random Forest, Neural Network (NN), Deep Learning, Support Vector Machine (SVM), Naïve Bayes block diagrams.

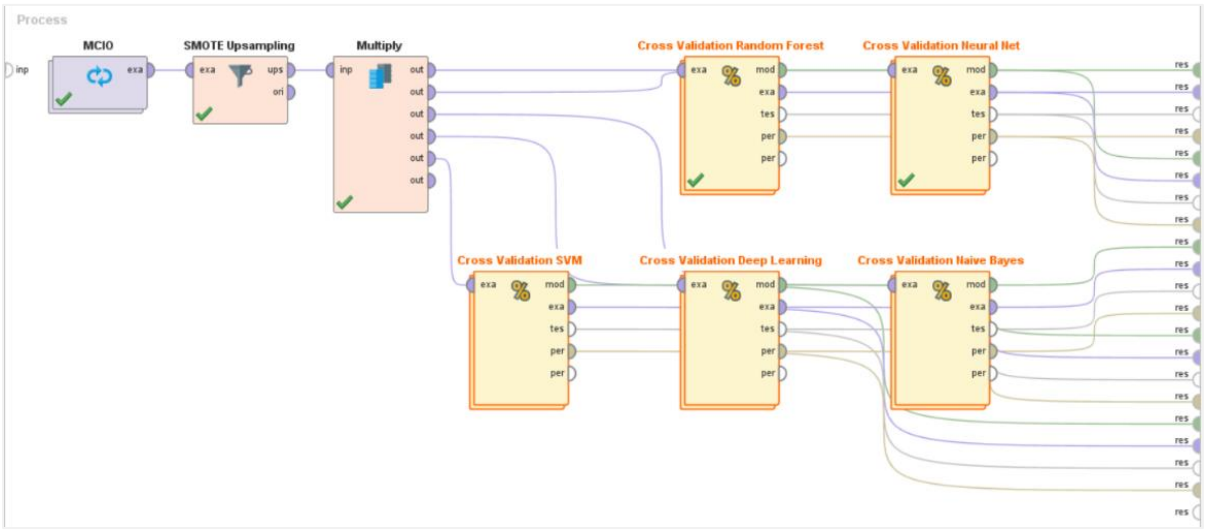

Figure 8: Block diagram for setting models parallelly by the Multiply operation

6.4 Validation setting

In this step, we used the data for making models and tested models obtained, called validation. The methods used for validation were split validation and cross-validation. For the split validation, 3 cases for ratios of training sets to testing sets were considered, 70%:30%, 75%:25%, and 80%:20%. All four methods were considered for performance evaluation.

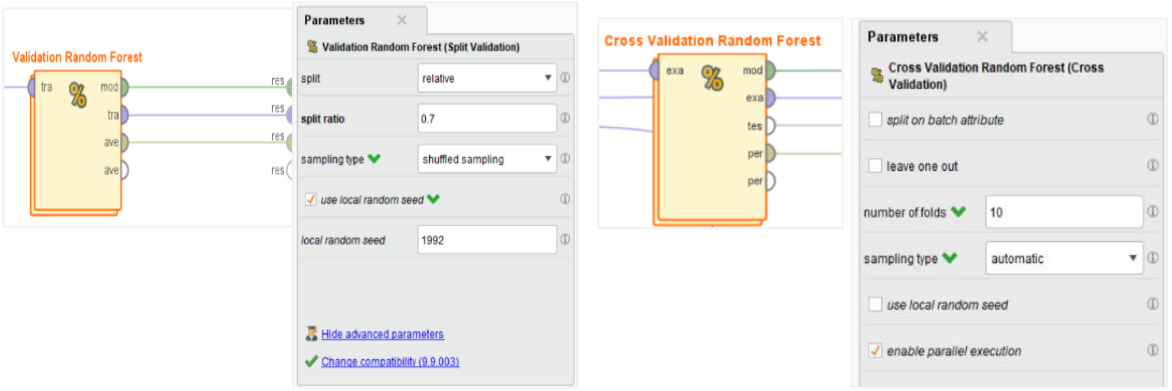

(a) (b)

Figure 9: Block diagram for setting parameters for validation
(a) split validation (b) cross-validation

6.5 Making models

In this part, all models of 5 algorithms with 4 methods of validation were created and evaluated the performance.

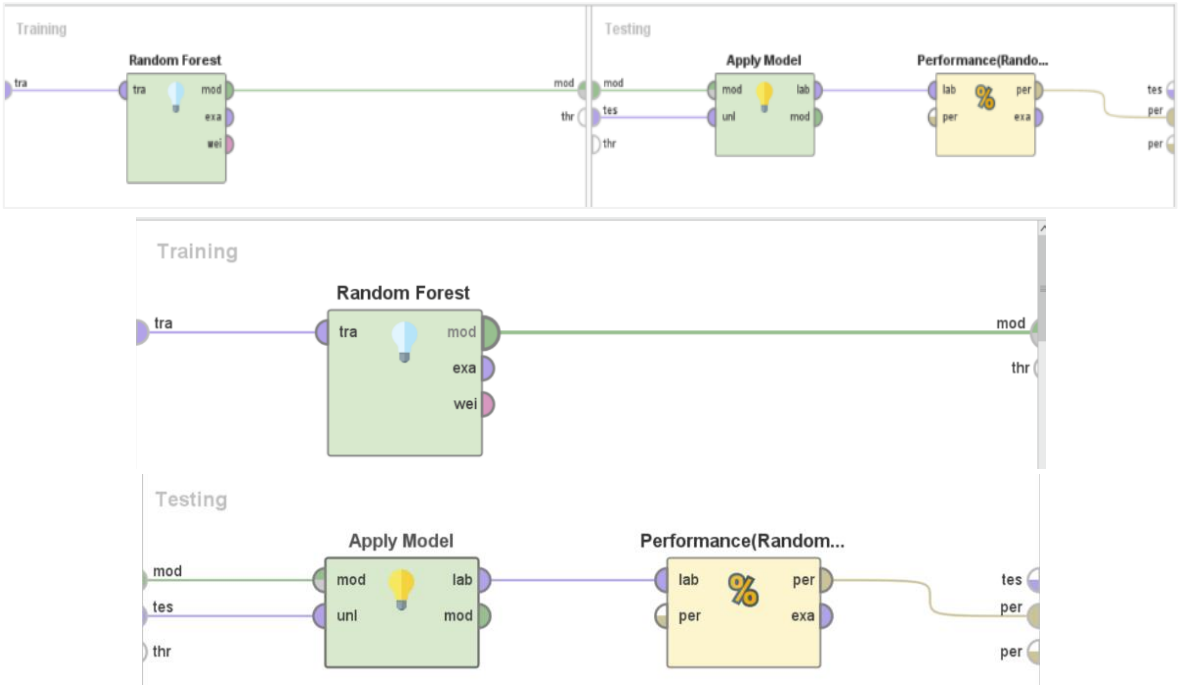

Figure 10: Example of a Block Diagram for Model Creating and Model Evaluation

7. Performance Evaluation

7.1 Results by using waveform files

Table 1: 70% Training and 30% Testing Split Validation

Method	Accuracy	Recall	Precision	F1-score
Random Forest	82.89%	77.50%	88.57%	82.67%
Neural Net	80.26%	62.50%	100.00%	76.92%
Deep Learning	82.89%	80.00%	86.49%	83.12%
Support Vector Machine	76.32%	65.00%	86.67%	74.29%
Naïve Bayes	78.00%	56.00%	100.00%	71.79%

Table 2: 75% Training and 25% Testing Split Validation

Method	Accuracy	Recall	Precision	F1-score
Random Forest	82.54%	78.79%	86.67%	82.54%
Neural Net	87.30%	78.79%	96.30%	86.67%
Deep Learning	80.95%	63.64%	100.00%	77.79%
Support Vector Machine	79.37%	69.70%	88.46%	77.97%
Naïve Bayes	78.00%	56.00%	100.00%	71.79%

Table 3: 80% Training and 20% Testing Split Validation

Method	Accuracy	Recall	Precision	F1-score
Random Forest	80.00%	84.00%	77.78%	80.77%
Neural Net	86.00%	72.00%	100.00%	83.72%
Deep Learning	88.00%	80.00%	95.24%	86.96%
Support Vector Machine	76.00%	72.00%	78.26%	75.00%
Naïve Bayes	78.00%	56.00%	100.00%	71.79%

Table 4: Cross-Validation

Method	Accuracy	Recall	Precision	F1-score
Random Forest*	86.20%	82.54%	88.89%	85.60%
Neural Net	83.74%	75.40%	90.48%	82.25%
Deep Learning	83.37%	76.98%	88.18%	82.20%
Support Vector Machine	77.37%	70.63%	81.65%	75.74%
Naïve Bayes	71.78%	46.03%	95.08%	62.03%

7.2 Results by using spectrogram of sound files

Table 5: 70% Training and 30% Testing Split Validation

Method	Accuracy	Recall	Precision	F1-score
Random Forest	92.11%	90.00%	91.74%	90.86%
Neural Net	81.58%	85.00%	80.95%	82.93%
Deep Learning	80.26%	75.00%	85.71%	80.00%
Support Vector Machine	75.00%	52.50%	100.00%	68.85%
Naïve Bayes	70.00%	44.00%	91.67%	59.46%

Table 6: 75% Training and 25% Testing Split Validation

Method	Accuracy	Recall	Precision	F1-score
Random Forest	92.06%	90.91%	93.75%	92.31%
Neural Net	74.60%	66.67%	81.48%	73.33%
Deep Learning	80.95%	48.48%	80.00%	60.37%
Support Vector Machine	73.02%	44.00%	100.00%	61.11%
Naïve Bayes	70.00%	44.00%	91.67%	59.46%

Table 7: 80% Training and 20% Testing Split Validation

Method	Accuracy	Recall	Precision	F1-score
Random Forest	92.00%	88.00%	95.65%	91.67%
Neural Net	88.00%	80.00%	95.24%	86.96%
Deep Learning	82.00%	84.00%	80.77%	82.35%
Support Vector Machine	74.00%	48.00%	100.00%	64.86%
Naïve Bayes	70.00%	44.00%	91.67%	59.46%

Table 8: Cross Validation

Method	Accuracy	Recall	Precision	F1-score
Random Forest*	93.69%*	89.68%*	97.41%*	93.39%*
Neural Net	86.89%	76.98%	96.04%	85.46%
Deep Learning	87.31%	83.33%	90.52%	86.78%
Support Vector Machine	75.78%	51.59%	100.00%	68.07%
Naïve Bayes	69.46%	48.41%	83.56%	61.30%

Remark *The model which had the highest performance.

Discussion

By the results proposed, we found that the Random Forest algorithm was the best one for sound classification. It provided the highest accuracy in almost all validations. For the validation of the model, the cross-validation technique always performed better than split validation. Random Forest algorithm also worked better in the classification of spectrogram compared to the classification of spectrogram waveform directly, which had accuracy, precision, and F1-score more than 90%.

Conclusion

It was found that the Random Forest technique with cross-validation of a spectrogram of sound files provided the best performance, which had accuracy = 93.69%, precision = 97.41%, recall = 89.68%, and F1-score = 93.39%.

Acknowledgment

This work was supported by Suranaree University of Technology One Research One Graduate scholarship (SUT OROG scholarship). We also want to express our sincere gratitude to the center of excellence in biomechanics medicine, school of biomedical innovation engineering, school of electric engineer, and school of mathematics, Suranaree University of Technology, Thailand.

References

Aktar, S. F., & Andrei, S. (2020). Detecting Heart Diseases using a Stethoscope-based Heart Sound Method. *ACET Journal of Computer Education & Research, 14*(1), 1-45.

Baydoun, M., Safatly, L., Ghaziri, H., & El Hajj, A. (2020). Analysis of heart sound anomalies using ensemble learning. *Biomedical Signal Processing and Control*, 62. 102019.

Bourouhou, A., Jilbab, A., Nacir, C., & Hammouch, A. (2020). Heart Sound Signals Segmentation and Multiclass Classification. *International Journal of Online & Biomedical Engineering, 16*(15), 64-79.

Chowdhury, M. E. H., Khandakar, A., Alzoubi, K., Mansoor, S., M. Tahir, A., Reaz, M. B. I., & Al-Emadi, N. (2019). Real-Time Smart-Digital Stethoscope System for Heart Diseases Monitoring. *Sensors*, *19*(12), 2781.

Schmitt, M. (2020). Artificial Intelligence in Medicine. Retrieved September 10, 2021, from https://www.datarevenue.com/en-blog/artificial-intelligence-in-medicine

Sittichanbuncha, Y. (2021). Artificial Intelligence (AI) and Its Use in Healthcare and Emergency Medicine. *Journal of Emergency Medical Services of Thailand*, *1*(1), 91-104.

Yang, L., Li, S., Zhang, Z., & Yang, X. (2020). Classification of phonocardiogram signals based on envelope optimization model and support vector machine. *Journal of Mechanics in Medicine and Biology*, *20*(01), 1950062.

Zhang, W., Han, J., & Deng, S. (2019). Abnormal heart sound detection using temporal quasi-periodic features and long short-term memory without segmentation. *Biomedical Signal Processing and Control*, *53*. 101560.

COST-EFFECTIVENESS PRODUCTIVITY IMPROVEMENT

Paritud Bhandhubanyong[1*] and Kyoko Kato[2]

[1]Faculty of Logistics and Transportation Management, Panyapiwat Institute of Management, Thailand
[2]College of Engineering and Design, Shibaura Institute of Technology, Japan
***Corresponding author, E-mail:** paritudbha@pim.ac.th

Abstract

The global spread out of COVID-19 is causing disruption in both manufacturing and service. Small and medium enterprise (SME) working in the supporting industry has been seriously affected by the abrupt demand change in the manufacturer of the finished goods. The keys to survival are agile and resiliency through continuous improvement. Management must develop a strategy to increase productivity with hardware, software, and human ware development. This is a long and difficult journey through a hands-on working spirit. Thai Metro Industry (TMI) is a family business specializing in roller chain manufacturer. In order to compete in the domestic and overseas market, the company applied Japanese management concepts with the aim to reduce wastages and losses in the processes. TMI practiced Toyota Production System (TPS) through the support of the public sector. In-house design and development of process automation and online quality inspection real-time report are beneficial for cost-effective productivity improvement.

Keywords: Cost, Productivity

Introduction

The world-renowned think-tank in Europe announced the 2022 risk outlook detailing the 10 scenarios that could affect global growth and inflation (BIZweekmu, 2021) Of all 10, the economic-related ones are about half of them which reflected the coming slow growth, if not recession, of the worldwide economy. Two of the higher probability and high to very high impact risks are; *Fast monetary tightening leads to the stock market crash* and *Tighter financial conditions derail a recovery in emerging markets.* In Thailand, a widely publicized economic research unit stated several economic risks that could affect the country to get stuck in the serious economic slowdown, namely, the lack of insufficient investment in R and D and innovation in the economic sectors (Jaiwat, 2021). The following paper about 9 months later advised that Thailand is losing the reveal comparative advantage especially in agricultural products to Vietnam starts to catch up very rapidly. This is due to the low productivity in the sector (Bhandhubanyong & Sirirungsri, 2020). The comparative study in the domestic agricultural sector revealed the benefit of ICT application coupled with farm mechanization in the agricultural sector that can improve productivity and, in turn, the comparative advantage of the sector (Bhandhubanyong & Sirirungsri, 2021).

Thai Metro Industry Co., Ltd. or TMI is one of the small and medium companies in the supply chain of the major overseas agricultural machine and equipment manufacturers. Over the nearly 5 decades of existence, the company started from a family business enjoying the production of standard and medium prices roller chain products supplied to the motorcycle assemblers and industrial customers. TMI faced serious financial problems when China started flooding the roller chain market with very low prices of standard products. Thus, begin the journey of the company to a global level manufacturer or from a “slum” to a “star” factory Kato and Bhandhubanyong (2018). This paper is a

follow-up on the continuous improvement of TMI and lessons learned for SMEs in Thailand in order to compete in the "no normal" future global market.

The Journey

TMI started the journey towards global level productivity due to two factors, severe competition in domestic and overseas markets, and, the strong will of Mr. Pipob Vivatanaprasert, Managing Director, who announced that:-

"We will manufacture high-quality products for a high-quality market. We aim to make better quality than Japanese products. Consequently, we emphasize on research and development (R&D) and continuous improvement or Kaizen for better quality, lower cost, 100% timely delivery, to achieve customer satisfaction."

A series of techniques, namely, 5S, suggestion system, ISO 9000, Toyota Production System (TPS), and Lost Reduction Process (LRP), have been applied consecutively with the strong support from the outside by the Thailand Automotive Institute (TAI), a unit under the Ministry of Industry (MOI) and the inside from all members of the workforces. The comment from the Global Problem-Based Learning participants after observing TMI factory operation strongly reflected the commitment to Kaizen or continuous improvement of the managers and the floor staff Thammasak and Nopparat (2021). The initial achieved targets were a 50% reduction of WIP and lead-time, a 30% reduction of working space, and a 30% improvement of effectiveness.

Cost-Effectiveness Hardware, Software, and Human ware Development at TMI

Since 2019, the Thai government announced the policy to achieve "Thailand 4.0" especially in the real sector. Various institutions operating under the Ministry of Industry have been entrusted with the tasks to support the private sector for this endeavor. This is not an easy task as the average level of the firms in the Thai industrial sector is at about 2.0+ level especially in the small and medium enterprises. Lack of qualified, well-trained technical people coupled with a lack of investment resources exemplified the problems further.

Recently, the Office of Industrial Economics of MOI reported that Thailand applies about 60 robots per 10,000 employees while the number is 112 robots per employee in South Korea and Singapore. Lack of system integrator made only 25% of Thai industry firms apply robotically and automation technology.

To improve productivity through hardware development, TMI applied in-house designed chain link assembly, which is one of the bottleneck processes. Figure 1 compared the manual machine with the automatic one.

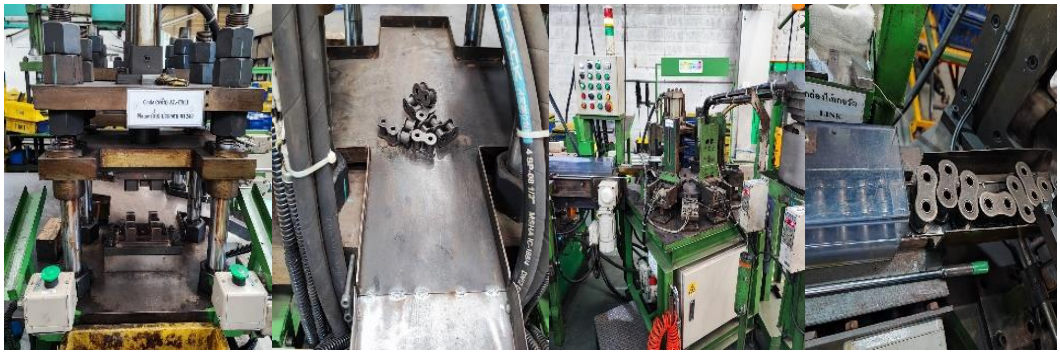

Figure 1: Chain Link Assembly Machine with output tray manual (Left) and Automatic (Right)

Quality inspection and control in the final chain assembly used to be done manually by hand measurement tools. The total length of the chain is a critical dimension. Histogram and Control Charts were applied through Loss Prevention Program or LRP. Process Capability Indices of Cp and Cpk were calculated and manually reported to justify the controllability of the process. These are rather time-consuming and error-prone. To alleviate these problems, TMI applied the in-line quality inspection with the application of software developed by university staff. Figure 2 shows the display of the in-line quality inspection outcomes.

	Type	No.	M/C	NB	Lot.	Xbar-std	Xbar	Cpk
1	RH	120D	BK3		17-11-12	38.10	38.100	3.096
2	RH	120D	BK3		17-11-11	38.10	38.106	13.160
3	RH	120D	BK3		17-11-10	38.10	38.104	6.580
4	RH	120D	BK3		17-11-09	38.10	38.088	4.785
5	RH	120D	BK3		17-11-08	38.10	38.089	3.290
6	RH	120D	BK3		17-11-07	38.10	38.079	3.096
7	RH	120D	BK3		17-11-06	38.10	38.093	3.509
8	RH	120D	BK3		17-11-05	38.10	38.090	5.264
9	RH	120D	BK3		17-11-04	38.10	38.083	8.773
10	RH	120D	BK3		17-11-03	38.10	38.092	2.771
11	RH	120D	BK3		17-11-02	38.10	38.100	2.106
12	RH	120D	BK3		17-11-01	38.10	38.092	4.049

Figure 2: In-line quality inspection outcomes exhibited a high value of Cpk

Human resources development is very crucial for productivity improvement. As previously reported, TMI applied various Japanese management techniques which mostly focused on the human side of the enterprise. Top-down to create bottom-up management is the key to the success of almost all the Japanese management techniques be it QCC, Suggestion System, Kaizen, TPS, etc. Generally speaking, employees working with his hand and heads will be more motivated than those working by top-down ordering alone. Since the beginning of the journey, TMI introduces a suggestion system and QCC through vigorous training of front-line operators and office personnel. Management by walking around (MBWA) is also a very effective way to observe and guide the operators to think and submit kaizen suggestion proposals and/or QCC topics. Table 1 shows the statistic of the number of monthly kaizen proposals for the past 4 years while figure 3 shows the example of the QCC case report.

Outcomes

After the achievement of the initial targets through TPS application, continuing productivity improvement through hardware, software, and human ware yield highly satisfactory outcomes. Before the application of automatic chain link assembly, the number of roller chain outputs per day was 150. With automatic assembly machines, the number increased to 380 or around 2.53 times with the same number of operators. Total cost reduction is around 25% by the overall productivity improvement.

TMI also can be able to keep the 5S condition well over the long years after the initial application. This is reflected by the cleanliness and tidiness of the factory as shown in Figure 4. As

Mr. Masuo Suyama, famous TQM for Problem Solving instructor used to say that the evidence of effective 5S is “straight line and perpendicular layout” on the shop floor. TMI can start and stop all the works in the factory and office on time with a very low rate of absenteeism and lateness for work. This is due to the practice of morning exercise and one-point talk (taking a turn by all operators and supervisors) before the beginning of the daily operation.

One more important observation point is that Mr. Pipob keeps allowing the overtime works for operators to support their income even if there is no need for satisfying the customer order. These overtime works, when there is no need for production operation, will be for 5S activities such as cleaning, and routine or autonomous maintenance of machines and equipment. The outcomes of these productivity improvement activities are more than offset the cost incurred by the overtime work.

Discussions

Human resources development can be clearly seen as an important factor for cost-effective productivity improvement at TMI reflected by the number of Kaizen proposals shown in Table1. The number has always been more than the target and almost all of the proposals could be applied with satisfactory results.

With the exception of major companies with a long history of active human resources development e.g. SCG PCL or Toyota Motor Corporation, the number of Kaizen proposals per employee per month of the Thai companies that applied the system are always far less than the number of employees.

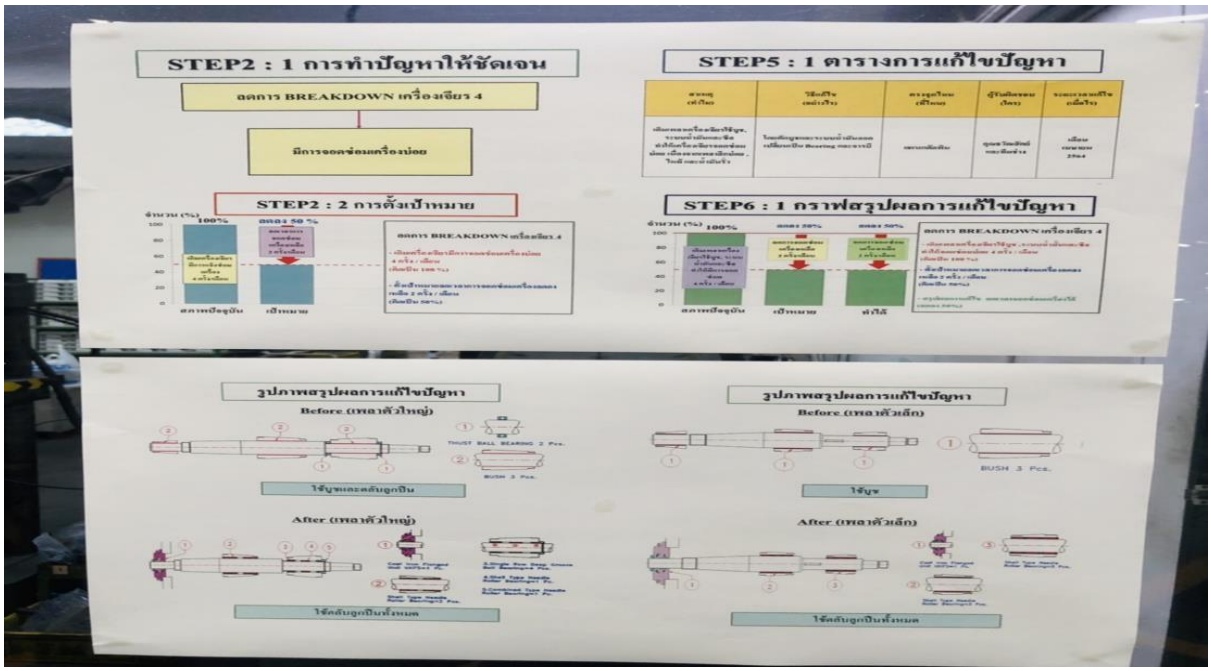

Figure 3: Example of QCC Case Report by a group of operators.

Figure 4: Cleanliness and tidiness of factory and stock area of finished goods (Rotary Chain)

Table 1: Number of monthly Kaizen proposals from the year 2017-2020 (Actual/Target)

year / month	2017	2018	2019	2020
January	10/10	92/50	65/55	65/47
February	10/10	53/50	65/51	65/47
March	11/10	57/50	61/55	61/46
April	12/10	66/65	79/51	79/46
May	10/10	96/56	80/53	80/46
June	16/15	120/58	74/51	74/50
July	22/15	120/60	72/53	72/46
August	50/50	120/58	72/55	72/45
September	103/50	111/58	70/55	70/45
October	60/50	120/56	57/53	57/46
November	87/50	85/56	64/53	64/44
December	54/50	84/56	67/53	67/44
Total	445	1124	905	826

Conclusions

Lesson learned or best practices of TMI that exhibited throughout the journey are 1) Continuous improvement through human resources development, 2) Top-down to create bottom-up with management by walking around practices by top management, managers, and supervisors, 3) In-house development of cost-effectiveness automated machine, 4) Application of in-line inspection reported for effective process control. The journey is rarely over and TMI will have to work

continuously in the so-called no normal situation towards the agile and resilient organization in the years to come.

References

Bhandhubanyong, P. & Sirirungsri, P. (2020). *Comparative Study of Non-ICT Supported Agricultural Supply Chain and ICT Supported Ones* (Research report), Bangkok: THA. Research Center, JETRO.

Bhandhubanyong, P., & Sirirungsri, P. (2021). The Pathway of Agricultural Supply Chain: Case Study of Thailand. *Proceeding* of *the 14th TSAE International 2021 Conference*, (1-13), May 24-26. Bangkok: TSAE.

BIZweekmu. (2021). *10 scenarios that could impact global growth and inflation.* Retrieved September 10, 2021, from *http://www.bizweek.mu/fr/info/10-scenarios-could-impact-global-growth-and-inflation*

Jaiwat, W. (2021). KKP Research reveals 3 risks that the Thai economy is stuck in If not close the gap in technology and innovation. Retrieved November 20, 202, from https://brandinside.asia/kkp-research-point-3-challenges-of-thai-equities-why-slow-recovery-11-nov-2020/

Kato, K., & Bhandhubanyong, P. (2018). *Global Problem-Based Learning with the collaboration of Thai and Japanese Universities/ Companies- Explaining the 3-year experiences of our Kaizen-PBL program development,* ISJET, *l2*(2), 12-20.

Thammasak, T. & Nopparat, N. (D.J.). (2021, November 19). *Econ Biz Program*. [Radio Broadcast]. Bangkok, Thailand: Radio 96.5.